

On the electrochemical intercalation of calcium and magnesium in TiS₂: fundamental studies related to multivalent battery applications

Deyana Tchitchekova^a, Alexandre Ponrouch^{a*}, Roberta Verrelli^a, Thibault Broux^a, Carlos Frontera^a,
Andrea Sorrentino^b, Fanny Barde^c, Neven Biskup^d, M.Elena Arroyo-de Dompablo^e and M.Rosa Palacín^{a*}

a. Institut de Ciència de Materials de Barcelona (ICMAB-CSIC), Campus UAB, E-08193 Bellaterra, Catalonia, Spain.

b. MISTRAL Beamline – Experiments Division, ALBA Synchrotron Light Source, Carrer de la Llum, 2-26, 08290 Cerdanyola del Vallès, Barcelona, Spain.

c. Toyota Motor Europe, Research & Development 3, Advanced Technology 1, Technical Centre, Hoge Wei 33 B, B-1930 Zaventem, Belgium.

d. Instituto Pluridisciplinar, Universidad Complutense de Madrid, 28040 Madrid, Spain.

e. Departamento de Química Inorgánica, Universidad Complutense de Madrid, 28040 Madrid, Spain.

ABSTRACT:

A comparative study of the electrochemical intercalation of Ca²⁺ and Mg²⁺ in layered TiS₂ using alkylcarbonate based electrolytes is reported and, for the first time, reversible electrochemical Ca²⁺ insertion is proved in this compound both using X-ray diffraction and differential absorption X-ray tomography at the Ca L₂ edge. Different new phases are formed upon M²⁺ insertion, that are structurally characterized, their amount and composition being dependent on M²⁺ and the experimental conditions. The first phase formed upon reduction is found to be the result of an ion-solvated intercalation mechanism, with solvent molecule(s) being co-intercalated with the M²⁺ cation. Upon further reduction, new non co-intercalated calcium containing phases seem to form to the expense of unreacted TiS₂. The calculated activation energies barriers for Ca²⁺ migration in TiS₂ (0.75 eV) are lower than those previously reported for Mg (1.14 eV) at the dilute limit and within the CdI₂ structural type. DFT results indicate that the expansion of the interlayer space lowers the energy barrier and favours a different pathway for Ca²⁺ migration.

Corresponding authors

* E-mail: aponrouch@icmab.es; rosa.palacin@icmab.es

Introduction:

The current energy related research context, involving imperative evolution towards electrification of transportation and renewable energy integration, challenges batteries to achieve maximum energy density at low cost while being environmentally friendly. Technologies based on the use of metal anodes and multivalent cations as charge carriers re-emerged as a field to explore^{1,2} with lessons learned from all developments made in the Li-ion battery field. For such technologies, the number of ions that must react to achieve a certain electrochemical capacity would diminish by a factor of two or three for bivalent or trivalent ions, respectively, or, for the same number of reacted ions, a concomitant two- or threefold increase in the energy density of the cells can be expected. The main caveat in this concept comes from the slow kinetics of the solid state diffusion of multivalent ions, which penalizes the expected power performance. This has been addressed by using more covalent hosts for insertion, which allowed proof of concept for a secondary magnesium metal based battery with the $\text{Mo}_6\text{S}_{8-\gamma}\text{Se}_\gamma$ ($\gamma=1,2$) Chevrel phases as positive electrodes.³ Further research enabled significant progresses, but commercialization has remained elusive due to some remaining technical bottlenecks such as the lack of a high energy density cathode and the complexity of the electrolytes developed.⁴ Research in analogous calcium metal based technologies is much more restricted, as the viability of reversible calcium metal plating and stripping was shown only very recently.⁵ The fact that conventional alkylcarbonate based electrolytes can be employed, provided a moderate temperature is used to mitigate tendency to ion pairing, prompted research on possible high potential cathodes such as CaMoO_3 or CaMn_2O_4 which unfortunately were found to exhibit too large energy barriers for calcium ion diffusion.^{6,7} Alternatively, V_2O_5 , Prussian blue related compounds operating at much lower potential or Ca ion exchanged Na_xCoO_2 have also been investigated either in primary systems or using different counter-electrodes, as the electrolytes used did not enable reversible calcium electrodeposition.^{8,9,10,11,12}

Research dealing with layered transition metal chalcogenides in general and TiS_2 in particular, laid the foundation of intercalation chemistry in the 70's.¹³ Their structural unit building block consists of two hexagonally close-packed chalcogenide layers between which reside the transition metal ions in either octahedral (as is the case of Ti(IV)) or prismatic sites. These building units are stacked together leaving a van der Waals gap in which intercalation of a range of neutral or charged species is possible, the latter concomitant to reduction of titanium. As far as we know, the first attempts to intercalate alkaline earth ions in TiS_2 were carried out independently by Schöllhorn *et al.*^{14,15} and Rouxel *et al.*¹⁶ by treating $\text{Na}_x(\text{H}_2\text{O})_y\text{TiS}_2$ ($x=0.5$) in 1 M aqueous solutions containing alkaline earth salts or using calcium metal in liquid ammonia,

respectively. Gregory *et al.*¹⁷ attempted to intercalate magnesium ions either chemically, using a 0.7 M solution of dibutyl-magnesium in heptane, or electrochemically, using a 1 M solution of $\text{Mg}(\text{ClO}_4)_2$ in THF, reporting in both cases the formation of $\text{Mg}_{0.15}\text{TiS}_2$ but with no detailed structural characterization. In contrast, decomposition and reduction to elemental sulphur was reported after similar electrochemical tests by Novak *et al.*¹⁸ Partial chemical reduction with bis(2,6-di-tert-butylphenoxide) was confirmed by Bruce *et al.*¹⁹ to yield a mixture of unreacted phase and Mg_xTiS_2 ($x \gg 0.22$), with a concomitant expansion of the *c* axis from 5.699 to 6.127 Å and possible co-intercalation of phenoxide related species. Further work by Amir *et al.*²⁰ reported *ca.* 20 mAhg^{-1} reversible capacity in electrochemical experiments using Mg metal counter electrodes and $\text{THF}/\text{Mg}(\text{AlCl}_2\text{BuEt})_2$ electrolytes at 60°C, but unfortunately no complementary characterization techniques were used to assess the structural changes associated, if any.

The above mentioned renewed interest in multivalent chemistries prompted at further studies, and Mg^{2+} intercalation into layered TiS_2 has been reported lately from all-phenyl-complex (APC)/THF electrolyte, with capacity of 270 mAhg^{-1} on first discharge at C/20 rate and 60°C.²¹ Upon subsequent oxidation only about 150 mAhg^{-1} were recovered, with significant capacity fade upon following cycles. This was attributed to Mg^{2+} trapping and complex ordering within the host structure, in agreement with density functional theory (DFT) calculations,²² pointing at irreversible transformations preventing the recovery of the pristine TiS_2 structure upon the first oxidation. The intercalation of MgCl^+ into interlayer-expanded TiS_2 at 25°C from APC/THF electrolyte with 0.2 M PY14Cl added was also recently reported.²³ In this case, despite recovery of the capacity upon re-oxidation, the pristine TiS_2 structure was not recovered either. Finally, an interesting $\text{Na}^+/\text{Mg}^{2+}$ hybrid-ion cell has been reported, with chemical reaction between layered TiS_2 and 1.0 M NaBH_4 + 0.1 M $\text{Mg}(\text{BH}_4)_2/\text{DGM}$ hybrid electrolyte taking place prior to electrochemical cycling.²⁴ Thus, none of the studies dealing with Mg^{2+} intercalation into TiS_2 reports full reversibility and recovery of the pristine TiS_2 framework.

In this paper we present a fundamental study comparing the electrochemical intercalation of divalent cations (Ca^{2+} and Mg^{2+}) in layered TiS_2 using alkyl carbonate based electrolytes. Their different charge to radius ratio resulting in different polarizing power is expected to affect both the interaction within the solid TiS_2 framework but also with the solvent molecules, which renders the comparison relevant from a fundamental research perspective. Thorough structural characterization from synchrotron X-ray diffraction of the phases formed experimentally is performed, and the reversibility of the redox process is ascertained. Ca^{2+} insertion inside the TiS_2 particles is further assessed by complementary differential absorption

X-ray tomography analysis. Energy barriers for Ca^{2+} diffusion are calculated by DFT. In the end, new research perspectives opened by these results are briefly discussed.

Methods

Experimental

Electrodes were prepared using commercial TiS_2 from Aldrich (purity 99.995%) as active material mixed with carbon black (Super P, Timcal, Switzerland) and polyvinylidene difluoride (Arkema) in weight ratios of 80:10:10. A slurry was made by dispersing the active material, carbon and binder powders in N-methyl-2-pyrrolidone (Aldrich, $\geq 99.9\%$), which was then ball milled for 2h, doctor blade casted on 18 μm thick aluminum foil (Goodfellow, 99%) and vacuum dried at 120°C for 3h. The tape was cut into discs of 11 mm diameter and pressed at 8 Tons before use.²⁵ Electrochemical tests were performed in three-electrode Swagelok cells using Ca metal (AlfaAesar, 99.5%) or Mg metal (AlfaAesar, 99.9%) as counter electrodes (CE) and reference electrodes (RE). This setup enables to independently follow the potential of the working (WE) and counter electrodes vs. the reference electrode and thus detect any side reaction at the CE that may in two electrode cells be misinterpreted as resulting from the WE. Representing the potential of the full cell $|E_{\text{WE}} - E_{\text{CE}}|$ enabled to illustrate the effect of the nucleation activation energy associated with the Ca plating on the CE on the full cell potential (see Results section). The electrolyte in Ca experiments was 0.45M $\text{Ca}(\text{BF}_4)_2$ dissolved in a 1:1 mixture of ethylene carbonate (EC) and propylene carbonate (PC) purchased from Solvionic (99.9%). In Mg cells, homemade dissolution of 0.3 M $\text{Mg}(\text{TFSI})_2$ (Solvionic, 99.5%) in a 1:1 mixture of EC (Aldrich anhydrous 99.0%) and PC (Aldrich anhydrous 99.7%) was prepared and used as electrolyte. A significant potential shift, of about 1 V or higher, has been reported for the Ca and Mg pseudo RE when operating in alkyl carbonate mixtures, namely the electrolytes used in this work, which strongly depends on the experimental conditions.²⁶ Thus, we have chosen not to correct the values and to report all electrochemical potentials vs. the appropriate pseudo RE, yet the upward shift has to be considered when comparing results with literature reports involving the use of APC/THF electrolytes. The water content in all the electrolytes was measured by Karl Fisher titration and found to be lower than 50 ppm in all cases. Electrolyte preparation and cell assembling were done in Ar filled glove box with less than 1 ppm of O_2 and H_2O . Prior to cycling, equilibration of the working electrode (WE) under the operating conditions at open circuit potential (OCP) was ensured. Cells were cycled using a Bio-Logic VMP3 potentiostat in either galvanostatic mode with potential limitation (GCPL) at rates ranging from C/50 to C/200 and various temperatures (100, 115°C) or by

potentiodynamic method (electrochemical potential spectroscopy, EPS),²⁷ also known as potentiodynamic cycling with galvanostatic acceleration (PCGA) at 100°C. The latter consists in scanning the potential with defined step amplitude (5 mV) for a duration limited by a current threshold ($C/200$ or $C/400$) in order to ensure full reactivity of the cathode at each potential step. The stability at OCP of the as prepared TiS_2 electrodes under our experimental conditions was ascertained by immersion in the corresponding Ca or Mg electrolytes inside two-electrode Swagelok cells for 30 to 100 hours at 100 and 115°C.

Synchrotron X-ray diffraction (SXR) patterns were collected at MSPD beamline of ALBA synchrotron using Mythen detector and $\lambda=0.6199$ Å. The samples, either pristine TiS_2 , or powder recovered from stability tests or cycled electrodes after dismantling the electrochemical cells inside Ar filled glove box, were embedded in a 0.5 mm diameter borosilicate glass capillary, and rotated during data collection.

Differential absorption tomography at Ca L_2 edge was acquired at Mistral beamline of ALBA synchrotron.^{28,29} Samples were transferred into the Mistral microscope chamber in dried N_2 atmosphere. The microscope was operating at -170°C. Data sets of two tomograms at 344.0 eV (Ca pre- L_2 edge) and 349.5 eV (Ca L_2 edge peak) were acquired with a constant effective pixel size of 11.8 nm. Transmission tilt series were collected from -54° to 54° with a 2° step. At each energy, 5 images were recorded with 3 seconds exposure time. To achieve precise alignment, it was necessary at each tilt angle to acquire an image stack at 344.0 eV followed by another at 349.5 eV. Transmission image stacks for each angle and energy were normalized with the flat field taking into account the electron beam current, averaged and converted to absorbance using the logarithm. The obtained absorbance tilt pairs (absorbance images at 344.0 and 349.5 eV at each angle) were aligned using EFTEM-TomoJ software³⁰ and the difference between them was calculated. The results are projections with a specific Ca signal which were manually aligned on the common rotation axis using IMOD.³¹ To reconstruct the 3D linear absorption coefficient the ART algorithm as implemented in TomoJ, with 15 iterations and a relaxation factor of 0.01, was used. The resulting tomogram has a voxel size of 11.8 x 11.8 x 11.8 nm³ and voxel signal equal to:

$$\mu_L(349.5 \text{ eV}) - \mu_L(344.0 \text{ eV}) = \rho(x,y,z) [\mu_m(349.5 \text{ eV}) - \mu_m(344.0 \text{ eV})]$$

where μ_L is the linear absorption coefficient, μ_m the mass absorption coefficient, ρ the material mass density and the x , y , z coordinates give the voxel position within the reconstructed volume. The above equation allows, assuming a specific Ca compound (*i.e.* CaCO_3 , CaF_2 or a given Ca_xTiS_2 intercalate) in a region of the reconstructed volume, to extrapolate the corresponding value for the mass density. The working principle of the method and its successful application to iron oxide nanoparticles mass density quantification in biological cells

were described by Conesa *et al.*³² Volume visualization, segmentation and analysis were performed using Chimera³³ and ImageJ.³⁴

Computational

First principle calculations have been performed using the *ab-initio* total energy and molecular dynamics program VASP (Vienna ab-initio simulation program) developed at the Universität Wien.³⁵ Total energy calculations based on Density Functional Theory (DFT) were performed within the General Gradient Approximation (GGA), with the exchange and correlation functional form developed by Perdew, Burke, and Ernzerhof (PBE)³⁶ and the adapted van der Waals potentials Opt-B86. The interaction of core electrons with the nuclei is described by the Projector Augmented Wave (PAW) method.³⁷ The energy cut off for the plane wave basis set was kept fix at a constant value of 500 eV throughout the calculations. The Ti ($3p^6, 3d^2, 4s^2$), S ($3s^2, 3p^4$), Ca ($3s^2, 3p^6, 4s^2$) and Sr ($4s^2, 4p^6, 5s^2$) were treated as valence states. The results presented here correspond to non-spin polarized calculations. Ca^{2+} mobility in layered TiS_2 and its dependence on the interlayer distance was investigated using the Nudged Elastic Band method (NEB)³⁸ as implemented in VASP. Activation barriers for Ca^{2+} migration in Ca_xTiS_2 were calculated at the dilute limit, $x \approx 0$, considering a $3 \times 3 \times 2$ supercell of the basic unit cell, where one Ca^{2+} is inserted in a vacant octahedral site. The two end-point configurations, in which Ca^{2+} reside in adjacent octahedral sites that are 3.39 Å apart, were fully relaxed. To examine the effect of the interlayer space on the energy barrier, the equilibrium structures were further distorted along the *c* axis by about 10% and 15%, allowing for internal atomic relaxations while the cell shape was kept fixed. Constant volume calculations were performed for five intermediate images initialized by linear interpolation between the two fully relaxed end points. To calculate the energy at the saddle point, cubic splines were fit through the images along each hop.

Results

Computational

In previous investigations of potential cathode materials for Ca batteries, we found that the electrochemical activity is hindered by impeded Ca^{2+} mobility. In particular, the calculated energy barriers for migration are as large as 1.8 eV for $CaMn_2O_4$ and 2 eV for $CaMoO_{3.6}$. Yet, the structural topology has been shown to have an effect in the expected multivalent cation mobility³⁹, and reasonable migration barriers have been predicted for some specific

frameworks. In the present work we have performed a DFT investigation of the Ca^{2+} diffusion behaviour in the layered TiS_2 structure (CdI₂ structure, S.G. $P\bar{3}m1$), with calculated lattice parameters $a=3.376$ Å and $c=5.704$ Å, in good agreement with the experimental values (see *Results-Characterization* section). When intercalation occurs, the intercalant ions enter the van der Waals gaps between the TiS_2 layers, where the available sites are the octahedral $1b$ (0 0 1/2) and the tetrahedral $2d$ (1/3 2/3 0.625). To investigate the energy barrier for Ca^{2+} migration in TiS_2 we have considered a single Ca^{2+} occupying an octahedral site in a $3 \times 3 \times 2$ supercell ($\text{CaTi}_{18}\text{S}_{36}$ or $\text{Ca}_{0.056}\text{TiS}_2$ composition), thus one intercalation layer remains empty (see figure S1 in Supplementary Information). As expected, the largest change produced by the intercalation is the expansion of the c lattice parameter with respect to the deintercalated structure. The insertion of a single ion led to the expansion of the interlayer space to ~ 6.84 Å, while the empty layer kept a distance of ~ 5.31 Å, with a total c axis length of 12.15 Å (compared to 11.41 Å in TiS_2).

Figure 1a shows the two possible pathways for the migration of Ca^{2+} in the ab plane of the TiS_2 structure. The simplest diffusion mechanism would imply the jump of Ca^{2+} from its octahedral site to an empty neighbouring octahedral site, across the common edge (path (i) in figure 1a). However, for Li^+ and Mg^{2+} insertion, the most favourable diffusion pathway from octahedral to octahedral site involves the intermediate occupation of the $2d$ tetrahedral site (path (ii) in figure 1a).^{22,40} For Ca^{2+} migration, we found that the direct interpolation of five images between the relaxed end-points favours path (i), with a calculated energy barrier of 0.75 eV. To calculate the barrier for Ca^{2+} migration along path (ii) it is necessary to interpolate images between the relaxed octahedral-site structure, $(\text{Ca}_{0.056})_{\text{Oh}}\text{TiS}_2$, and the relaxed tetrahedral-site structure $(\text{Ca}_{0.056})_{\text{Th}}\text{TiS}_2$. However, relaxation of $(\text{Ca}_{0.056})_{\text{Th}}\text{TiS}_2$ indicate that Ca^{2+} ions are not stable in the tetrahedral site; the single Ca^{2+} relaxes into the adjacent empty octahedral site. Further attempts to study path (ii), involving the interpolation of eleven images within the two relaxed octahedral-site end-points passing across the unrelaxed tetrahedral-site structure, did not reach convergence. Unsurprisingly, the tetrahedral site in the $\text{Ca}_{0.056}\text{TiS}_2$ structure is too small to accommodate the migrating Ca^{2+} , in contrast to what happens for the smaller Li^+ and Mg^{2+} cations. Indeed, additional calculations (see figure S1 in Supplementary Information) show that the occupation of the tetrahedral $2d$ sites by Ca^{2+} would require a notorious expansion of the c lattice parameter (from 5.70 Å in TiS_2 to 6.50 Å in $\text{Ca}_{\text{Oh}}\text{TiS}_2$ and 7.05 Å in $\text{Ca}_{\text{Th}}\text{TiS}_2$).

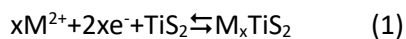
Several DFT studies demonstrated the general trend, that in layered structures the expansion of the interlayer space lowers the activation barriers for the intercalant ion migration, for instance in Mg_xTiS_2 ,²² Li_x -graphite,⁴¹ or Li_xMO_2 .⁴² In the present work we found that the energy

barrier of the equilibrium structure (0.75 eV) decreases to 0.48 and 0.41 eV, respectively, for 10% and 15% expansion of the *c* lattice parameter. The calculated energy barriers are shown in figure 1b, and the Ca²⁺ pathways in figure S2 of Supplementary Information. Interestingly, and in line with the above discussion, the *c* lattice expansion facilitates the Ca²⁺ migration across the larger tetrahedral site, and path (ii) becomes more favourable than path (i).

In summary, the calculated activation barriers for Ca²⁺ migration suggest that the intercalation of Ca²⁺ in the TiS₂ structure is feasible, with the kinetics of the reaction being strongly dependent on the interlayer space expansion. It is worth mentioning, that the calculated energy barrier for Ca²⁺ diffusion is lower than the value reported for Mg²⁺ (1.14 eV in the dilute limit Mg_{0.03}TiS₂).²² To assess the decreasing trend of the energy barrier with the alkaline earth cation size, we calculated the barrier for Sr²⁺ diffusion in the relaxed structure of Sr_{0.056}TiS₂ presenting interlayer distances of 7.26 Å for the inserted layer and 5.43 Å for the empty layer (*c*=12.67 Å). The calculated energy value is 0.5 eV, supporting that the larger intercalant size/less polarizing character of the divalent ion is, the lower the barrier is. These results are consistent with a recent DFT work by Samad *et al.*,⁴³ who found the same trend for Be, Mg and Ca diffusion on the surface of TiS₂ monolayers.

Experimental

The electrochemical intercalation of M²⁺ (divalent cation) in TiS₂ can be expressed as:



with charge being compensated by partial reduction of Ti(IV). The theoretical specific capacity for this system, when considering the intercalation of 1 mole of M²⁺ per mole of active material, is about 479 mAhg⁻¹. We investigated the electrochemical performance of TiS₂ in conventional alkylcarbonate electrolytes under different experimental protocols in Ca and Mg cells, as described in the experimental section. Unfortunately, Mg plating does not occur in the electrolyte used in this study (0.3 M Mg(TFSI)₂ in EC:PC), which prevents from investigating the possible reversibility of the Mg²⁺ intercalation. Results of Ca²⁺ insertion/deinsertion and Mg²⁺ insertion are displayed in figure 2, the recorded voltage profiles being reported vs. the corresponding Ca or Mg pseudo RE (see *Methods-Experimental* section).

Cyclic voltammetry (CV at scan rate 0.1 mVs⁻¹) of a TiS₂ electrode in Ca cell operating at 100°C is shown in figure 2a. At least two reduction peaks at *ca.* 1.43 and 1.87 V are observable, and the corresponding oxidation peaks appear at *ca.* 1.52 and 2.22 V vs. the Ca pseudo RE. The potential differences between the anodic and cathodic peaks are *ca.* 90 and 350 mV for the first and second waves, respectively, pointing at slow kinetics for the processes involved. Upon further cycling both reduction and oxidation waves change in shape, becoming broader and

shifting progressively towards higher voltages, reaching *ca.* 1.55 and 2.1 V upon reduction, and *ca.* 1.67 and 2.38 V upon oxidation in cycle 7. Galvanostatic experiments yield consistent results. The **potential versus composition profiles for some galvanostatic experiments** carried out at 100°C in Ca cells at different C rates (C/200, C/100 and C/50) are presented in figure 2b. Large pseudo-plateaus are observed in all cases **upon reduction**, centred at about 1.2, 1.45 and 1.5 V vs. Ca pseudo RE, respectively for experiments at C/50, C/100 and C/200 rates. The values at the slower C rates compare well with the potential of 1.43 V for the second reduction peak seen in the CV experiment. Specific capacities associated with these pseudo plateaus were also found to strongly depend on the C rate and 520 and 210 mAhg⁻¹ are achieved at C/100 and C/50, respectively. The experiment at C/200 has been stopped before the end of the plateau and the cell disassembled for diffraction measurements, however from the voltage profile it is clear that a capacity larger than 500 mAhg⁻¹ would be achieved upon reduction to 1 V. The reduction curves at C/200 and C/100 (blue and black curves) exhibit a small plateau (*ca.* 40 mAhg⁻¹) at 1.75 V vs. Ca pseudo RE, consistent with the first reduction peak seen in the CV experiment (figure 2a), which is missing at higher rate (C/50, orange curve) possibly due to slower kinetics. **When further oxidation is attempted**, significant voltage hysteresis is observed (ranging from 1.5 V up to 2.3 V at C/100 and C/50 rates respectively). This behaviour reflects the very slow diffusion of the Ca²⁺ ions (in the TiS₂ lattice and/or within the electrolyte) and/or the slow charge transfer kinetics. For comparison, GCPL experiments at C/50 rate run at 115°C were conducted and a typical first cycle is also shown in figure 2b (pink curve). The capacity achieved at C/50 (410 mAhg⁻¹) at this temperature almost doubles the value achieved at 100°C for the same C rate. The reduction curve shows a small plateau at 1.78 V vs. Ca pseudo RE and a subsequent large pseudo-plateau centred at 1.5 V vs. Ca pseudo RE. A voltage hysteresis of about 1.3 V is still observable. **It is worth mentioning that the peak observed in the voltage profiles upon oxidation only appears when the potential of the working electrode is represented vs that of the counter-electrodes (potentials in figure 2b refer to |E_{WE}-E_{CE}| in order to highlight this aspect).** Therefore, this peak upon oxidation is most probably related to a nucleation activation energy associated with the Ca plating on the CE and it is thus not related to the TiS₂ characteristic redox behaviour.

Galvanostatic reduction of TiS₂ in Mg cells using 0.3 M Mg(TFSI)₂ in EC:PC as electrolyte was carried out at 100°C. **Given the large potential shift of Mg pseudo-reference electrode in alkylcarbonate based electrolytes²⁶ (*ca.* 1V), the reduction was performed down to -0.7 V vs. Mg pseudo RE. The potential vs capacity profile** at C/100 is depicted in figure 2c (red), the specific capacity is *ca.* 70 mAhg⁻¹, corresponding to less than 0.2 mole of Mg²⁺ inserted. PCGA tests with current thresholds set at C/200 and C/400 were also carried out and characteristic

PCGA curves, displayed in figure 2c, show that much larger specific capacities of 290 and 500 mAhg⁻¹, respectively, can be achieved. The reduction of TiS₂ exhibits sharp changes in the potential profile up to about 60-70 mAhg⁻¹ that might be related to the formation of intercalation stages, followed by a sloping voltage decrease suggesting the formation of a solid solution. It is worth noting that the potential profiles upon galvanostatic and PCGA cycling in our experimental conditions differ from those obtained by Sun *et al.*²¹ in APC/THF electrolyte and 60°C, which are closer to the theoretical voltage curve calculated by Emly *et al.*²² for the Mg_xTiS₂ system using O1 stacking of the chalcogenide layers. This suggests that the redox mechanism observed in our work is different from what has been previously reported, as will be further interpreted in the *Discussion* section.

The SXRD pattern corresponding to the pristine TiS₂ tape electrodes used for electrochemical tests can be indexed in the $P\bar{3}m1$ space group with cell parameters $a=3.406(1)$ Å and $c=5.700(2)$ Å, in good agreement with the literature,⁴⁴ and no changes are observed for electrodes that have been immersed in the corresponding magnesium or calcium based electrolytes at 100 and 115°C, which indicates both that TiS₂ is stable in such conditions and that spontaneous solvent intercalation does not occur.

Several SXRD patterns corresponding to electrodes recovered from either Mg or Ca cells after different levels of reduction are displayed in figure 3 for Mg (top) and for Ca (bottom). For clarity, the capacity achieved upon reduction for each sample is specified next to the corresponding XRD pattern together with labels referring to the electrochemical curves in figure 2b (labels F and G) and in figure 2c (labels A, B and C). Labels D and E in bottom panel of figure 3 correspond to samples at intermediate stages of reduction in Ca cells, and the electrochemical curves have not been displayed in figure 2b for easier reading. Depending on the level of reduction and the cation inserted, mixtures of different phases are observed, together with low intensity peaks corresponding to CaF₂, most likely formed from electrolyte decomposition.

The first phase observed upon reduction (denoted as Phase 1 in figure 3) in both Ca and Mg cells is characterized by a very intense peak at $Q=0.673$ Å⁻¹ and $Q=0.668$ Å⁻¹ (corresponding to $d=9.34$ Å and $d=9.41$ Å) respectively, which seems to grow upon reduction to the expense of peaks corresponding to TiS₂. The peak set of Phase 1 can be indexed using a large hexagonal unit cell in the $R\bar{3}m$ space group. Cell parameters are $a=3.418(1)$ Å, $c=28.236(1)$ Å and $a=3.417(2)$ Å, $c=28.040(1)$ Å for the samples containing

Mg²⁺ and Ca²⁺, respectively. Similar cell parameters have already been reported for TiS₂ intercalates. For example Chianelli *et al.* reported (NH₃)TiS₂ with cell parameters $a=3.427(2)$ Å, $c=26.55(2)$ Å with two possible space groups $R\bar{3}m$ and $R3m$,⁴⁵ Mc Kelvy *et al.* reported several Li_x(NH₃)_yTiS₂ co-intercalated phases with a c cell parameter varying from 26.1 to 26.7 Å as a function of the amount of intercalated species⁴⁶ assuming a 3R type structure ($R\bar{3}m$ or $R3m$ space group) and finally the structure of Li⁺_{0.23}(ND₃)_{0.63}TiS₂ was determined by neutron powder diffraction using $R\bar{3}m$ space group.⁴⁷ In our case, refinement of the crystal structure has been attempted using $R\bar{3}m$ and $R3m$ space groups for the patterns A and D in figure 3, corresponding to electrodes reduced in Mg and Ca cells and delivering 70 mAhg⁻¹ and 160 mAhg⁻¹ capacities, respectively. The structural model used to describe the Phase 1 is similar to the one previously reported for Li⁺_{0.23}(ND₃)_{0.63}TiS₂, and $R\bar{3}m$ space group is chosen as it leads to better agreement factors ($R_{\text{Bragg}}=2.43$ and 3.74 for the $R\bar{3}m$ and $R3m$ space groups, respectively). The interlayer distances are equivalent to $c/3$, *i.e.* around 9.4 Å in both cases, and thus much larger than in the pristine TiS₂, in agreement with co-intercalation of both solvent molecules and cations.

As mentioned in the introductory section, intercalation of neutral or charged species in the van der Waals gap of TiS₂ is well known.^{24,48,49,50} Concomitant ion and solvent intercalation has also been reported, with interesting cases such as lithium and ammonia co-intercalated TiS₂ that contains NH₄⁺ ions along with NH₃ molecules acting as solvate for Li⁺.⁴⁶ More recently,²⁴ ageing of TiS₂ in diglyme based electrolytes with NaBH₄ as salt in absence of applied current was also shown to lead to the formation of several intercalates. In our experiments, the TiS₂ electrodes stored in the EC:PC (1:1 mixture) based electrolytes and Mg(TFSI)₂ or Ca(BF₄)₂ salts remain unchanged in absence of applied current, which indicates that the new phases observed during the reduction tests arise as a consequence of the electrochemical processes taking place.

While the solvent co-intercalation is not surprising, the presence of co-intercalated solvent molecules prevents the full elucidation of the structural model, which hampers proper estimation of the intensities of the Bragg peaks. This is in agreement with unreasonable atomic displacement parameters obtained for Mg and Ca when considering the formation of a non-solvated intercalant (see Table S1 in Supplementary Information), although the structural description for the titanium sulphide layer seems to be reliable in terms of interatomic distances. This result and the similarity between the two phases formed upon electrochemical reduction in Ca and Mg cells is also in full agreement with solvent molecules being co-intercalated with the corresponding cation M²⁺.

After the formation of this co-intercalated phase, further reduction of TiS_2 leads to different behaviours in Mg and Ca cells. In the Mg case the amount of the co-intercalated phase increases upon reduction to the expense of the amount of pristine TiS_2 and no other phases are seen in the pattern, with the exception of a small peak at $Q=0.896 \text{ \AA}^{-1}$ ($d=7.01 \text{ \AA}$), appearing after full reduction (500 mAHg^{-1}). In the case of Ca, larger capacities are achieved upon reduction at faster C rates, and the formation of two additional phases, denoted as Phase 2 and Phase 3 in figure 3, is observed. These new phases can be indexed in the $R \bar{3}m$ space group with the cell parameters $a=3.437(1) \text{ \AA}$, $c=21.073(2) \text{ \AA}$ and $a=3.419(1) \text{ \AA}$, $c=38.247(2) \text{ \AA}$, respectively. Cell parameters of Phase 2 are similar to $\text{Ca}_{0.5}\text{TiS}_2$, previously reported by le Blanc-Soreau *et al.*¹⁶ It was prepared via chemical reaction between TiS_2 and a solution of calcium in liquid ammonia to form $\text{Ca}_x(\text{NH}_3)_y\text{TiS}_2$, with Ca in prismatic coordination, which was subsequently heated to remove the co-intercalated ammonia. The pure $\text{Ca}_{0.5}\text{TiS}_2$ intercalate was found to crystallize in the $R \bar{3}m$ space group with cell parameters $a=3.444(4) \text{ \AA}$, $c=20.06(4) \text{ \AA}$, and with Ca^{2+} in octahedral coordination. In our case, assuming an octahedral coordination for Ca^{2+} leads to poor Rietveld refinement. Besides, simulated XRD patterns for both configurations (see figure S3 in Supplementary Information) indicate that the prismatic coordination is more consistent with our data for Phase 2, which would indicate layer shearing perpendicular to the c axis with respect to pristine TiS_2 . This is also supported by a recent theoretical investigation of the stability of prismatic and octahedral coordination in layered compounds,⁵¹ where the authors predicted that at intermediate concentrations of Ca^{2+} insertion in TiS_2 the P3 structure would be favoured. The cell parameters of Phase 3 are comparable with $\text{Na}_{0.3}\text{TiS}_2$ reported by Bouwmeester *et al.*⁵² $\text{Na}_{0.3}\text{TiS}_2$ crystallizes in the $R \bar{3}m$ space group with $a=3.406 \text{ \AA}$, $c=38.2 \text{ \AA}$ and corresponds to a second-stage intercalated structure. Our Phase 3 could be characterized using the same structure and the cell parameters $a=3.419(1) \text{ \AA}$, $c=38.247(2) \text{ \AA}$, and two significantly different interlayer distances for the empty (5.85 \AA) and intercalated (6.90 \AA) slabs, as depicted in the refined model of figure 3 (bottom). The calculated interlayer distance for Phase 3 (6.90 \AA) is much smaller than for Phase 1 (9.34 \AA), conforming to absence of solvent co-intercalation. Indeed, a rough estimate of the solvent molecule size gives about $3.8\text{-}4 \text{ \AA}$ for the EC ring and about $6\text{-}6.2 \text{ \AA}$ for PC. In addition, a distance for $S_L\text{-Ca}^{2+}$ ($S_L=\text{EC}, \text{PC}$) of nearly 2 \AA should be added to the S_L -molecule size.⁵³ These considerations altogether seem to indicate that Phase 3 is not a solvated- Ca^{2+} intercalate. It is also worth mentioning that this phase exhibits a clear split of the (006) reflection indicating the presence of more than one phase with subtle structural differences. The microstructures of these two phases are strongly different since the reflection at higher Q range is significantly broader than the one at lower Q . In spite of that, Rietveld refinement was

attempted considering a layered structure with stages, and thus two interlayer distances, corresponding to empty and intercalated slabs. The positions of titanium and sulphide ions have been determined, but unfortunately no reliable occupation factor for calcium could be achieved.

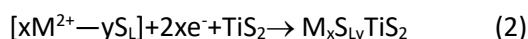
The X-ray diffraction pattern for a sample that has been fully reduced and re-oxidized in a calcium cell is also shown in figure 3 (pattern G). After oxidation of (co-)intercalated TiS_2 the initial structure is recovered. The broadening of the peaks indicates microstructural changes during the insertion and deinsertion processes. This confirms the full reversibility of the redox process with deintercalation of all the interlayer species upon oxidation.

Since reliable occupation factors for calcium haven't been achieved by Rietveld refinement of SXRD data of the reduced electrodes, and thus there is no direct assessment of the presence of Ca^{2+} in the TiS_2 interlayer space, Ca L_2 -edge differential absorption X-ray tomography was carried out on a particle from a reduced electrode (corresponding to pattern E in figure 3) operated in Ca cell (115°C and C/50 rate, 0.45 M $\text{Ca}(\text{BF}_4)_2$ in EC:PC, reduced to 1.25 V vs Ca pseudo RE with 410 mAhg^{-1} capacity). The method allowed reconstructing the 3D distribution of $\Delta\mu = \mu_L(349.5 \text{ eV}) - \mu_L(344.0 \text{ eV})$ in a $6.9 \times 10.9 \times 4.1 \text{ }\mu\text{m}^3$ volume, with a calculated sensibility of $0.21 \text{ }\mu\text{m}^{-1}$ (see figure S4 in Supplementary Information). Figure 4 shows the corresponding volumetric representation of the Ca distribution (voxels with $\Delta\mu > 0.21 \text{ }\mu\text{m}^{-1}$) outside (orange and red voxels) and inside (pink voxels) the reduced TiS_2 particle. The red region has a mean $\Delta\mu = 3.2 \pm 0.9 \text{ }\mu\text{m}^{-1}$, compatible with the theoretical absorption coefficient of CaCO_3 , and is named "high absorption external Ca" in figure 4. A "low absorption external Ca" with $\Delta\mu = 1.0 \pm 0.3 \text{ }\mu\text{m}^{-1}$ was also identified (orange voxels), and is tentatively ascribed to a polymeric film associated with the surface layer formed upon the first reduction of TiS_2 . Finally, a third Ca contribution was evidenced inside the TiS_2 particle (pink voxels) and is thus denoted as "intercalated Ca" with $\Delta\mu = 0.4 \pm 0.1 \text{ }\mu\text{m}^{-1}$. Assuming the crystalline structure of Phase 1 with formula either $\text{Ca}_{0.2}\text{TiS}_2$ or $(\text{Ca-S}_L)_{0.2}\text{TiS}_2$ ($S_L = \text{EC, PC}$), the theoretical mass densities of these intercalates are *ca.* 2.11 and up to 2.47 g/cm^3 (depending on S_L), respectively. The expected variation of the linear absorption coefficient is $\Delta\mu = 0.43 \text{ }\mu\text{m}^{-1}$ for the $\text{Ca}_{0.2}\text{TiS}_2$ intercalate and $\Delta\mu = 0.41\text{-}0.42 \text{ }\mu\text{m}^{-1}$ for the $(\text{Ca-S}_L)_{0.2}\text{TiS}_2$, all in perfect agreement with the experimental value measured by tomographic reconstruction for the "intercalated Ca". If we consider a higher x value for this phase, $\Delta\mu$ increases quickly, and already at $\text{Ca}_{0.25}\text{TiS}_2$ and $(\text{Ca-S}_L)_{0.25}\text{TiS}_2$ compositions, the corresponding theoretical variations of the linear absorption coefficient would be 0.57 and 0.54 μm^{-1} , respectively. Since the SXRD pattern of this sample shows similar intensities for the main peaks of Phases 1 and 2, as well as a very low intensity peak from

Phase 3, we have also verified the theoretical $\Delta\mu$ values for the possible $\text{Ca}_{0.5}\text{TiS}_2$ intercalate with crystalline structure of Phase 2 (theoretical mass density 3.05 g/cm^3 and $\Delta\mu=1.66 \text{ } \mu\text{m}^{-1}$) and the $\text{Ca}_{0.16}\text{TiS}_2$ intercalate with crystalline structure of Phase 3 (theoretical mass density 1.53 g/cm^3 and $\Delta\mu=0.25 \text{ } \mu\text{m}^{-1}$). Obviously, the theoretical $\Delta\mu$ for Phase 2 is too high and thus inconsistent with our experimental value, while the theoretical value for Phase 3 is too low, and probably at the limit of sensitivity of this technique. These findings suggest that in this reduced- TiS_2 particle, the amount of intercalated calcium ions is about 0.2 and it corresponds to Phase 1. To the best of our knowledge these results are the first unambiguous evidence for electrochemical Ca^{2+} intercalation into TiS_2 .

Discussion

SXRD results on TiS_2 electrodes reduced in EC:PC based electrolytes indicate that reduction in presence of divalent cations (M^{2+}) first yields Phase 1 resulting from the intercalation of solvated- M^{2+} ions, according to the following reaction:



with S_L being used as generic notation for EC and PC. This phase retains the same layered structure as the pristine TiS_2 but with a considerable expansion of the lattice along the c axis (interlayer distance $d=9.34 \text{ \AA}$), caused by the presence of solvent molecules. A significant amount of unreacted pristine TiS_2 is always observed, which is in agreement with the reaction above exhibiting slow kinetics, in line with DFT results showing high energy barriers for Ca and Mg migration. Indeed, the amount of remaining TiS_2 is smaller when using PCGA protocols with low limiting currents (C/400). When similar protocols are used, less unreacted TiS_2 is observed for Ca^{2+} than for Mg^{2+} containing electrolytes. In absence of additional redox phenomena an average x value can be deduced from the electrochemical capacity and if unreacted TiS_2 remains in the electrode the real amount of ions in the intercalated phases will be always higher than this average x . Yet, this cannot be taken for granted as some electrolyte decomposition can be expected at low potential as side reaction⁵, as in lithium and sodium cells using similar electrolyte formulations⁵⁴ and hence the value of x is overestimated. Within this scenario, the composition of the intercalated phases is somewhat uncertain although some information can be deduced from the results derived from SXRD and tomography. As an example, the fact that the SXRD pattern of a sample reduced in Mg cell (pattern B in figure 3) with electrochemical capacity of *ca.* 290 mAhg^{-1} (average $x\approx 0.6$) exhibit the presence Phase 1

($\text{Mg}_x\text{S}_y\text{TiS}_2$) together with a large amount of unreacted TiS_2 would indicate $x > 0.6$ for this phase, which is most certainly overestimated considering electrolyte reduction at low potential. For reduced electrodes in Ca cells with discharge capacities of *ca.* 300 mAhg^{-1} the composition of the Phase 1 is even more difficult to assess as some amounts of Phases 2 and 3 may have already formed.

Upon further reduction, (average $x \approx 0.85$) formation of Phase 2 is readily observed in Ca experiments and SXR (pattern E in figure 3) still indicates the presence of some unreacted TiS_2 together with Phase 1 with the low angle peak exhibiting similar intensities for the three phases. The interlayer distance for Phase 2 is 7.02 Å, which may be too low to accommodate a significant amount of solvent molecules. However, the slightly higher *c* cell parameter (21.07 Å) than the one reported for $\text{Ca}_{0.5}\text{TiS}_2$ (20.06 Å)¹⁶ may be compatible with minor amount of solvent molecules in the interlayer space. Thus, the formation of Phase 2 from Phase 1 seems highly unlikely, and we believe that Phase 2 forms at lower potentials to the expense of unreacted TiS_2 . The formation of Phase 2 seems to be largely inhibited for Mg^{2+} containing electrolytes. Basing on the hypothesis above that Phase 2 formed in Ca cells may not contain solvent and thus would form by intercalation of naked Ca^{2+} ions (with probably $x \approx 0.5$), one can speculate that Phase 2 is not forming in Mg cells due to higher solvation energy for the Mg^{2+} cations. This difference between Ca^{2+} and Mg^{2+} insertion mechanism may be rationalized through the higher polarizing character of Mg^{2+} as compared to Ca^{2+} , leading to stronger interaction with the solvent molecules. The larger $S_L\text{-Mg}^{2+}$ interaction than $S_L\text{-Ca}^{2+}$ has recently been illustrated by means of Raman spectroscopy using also EC:PC as electrolyte solvent²⁶ and is in agreement with theoretical calculations.⁵³

Relevant amounts of Phase 3 are only observed for very reduced electrodes in Ca^{2+} containing electrolytes (average $x > 0.9$). Since this phase seems to correspond to a second-stage intercalated TiS_2 (in agreement with cell parameter being very close to that of $\text{Na}_{0.3}\text{TiS}_2$), one can speculate that x for this phase is close to 0.3 and that its formation again arises from unreacted pristine TiS_2 and not from Phase 1 or Phase 2, as diffusion of ions through the chalcogenide slabs is not possible. The fact that its formation seems hindered for Mg^{2+} containing electrolytes is again in agreement with differences in solvation energy impeding intercalation of naked Mg^{2+} ions. The reasons favouring the alternative formation of Phases 2 or 3 in Ca^{2+} containing electrolytes remain unclear.

As already mentioned, reversibility of the redox process in Mg cells cannot be ascertained with the electrolyte used as it does not enable magnesium plating. However, our results confirm

that, despite the existence of side reactions involving electrolyte decomposition, reversible intercalation of *ca.* 0.5 mol of Ca²⁺ in TiS₂, with its microstructure being modified after the intercalation/deintercalation process. This behaviour is markedly different from the one reported for Mg²⁺ intercalation in TiS₂ using APC/THF,²¹ as significant Mg²⁺ trapping within TiS₂ structure was evidenced (about 0.26 mole), despite no solvent co-intercalation being mentioned.

From these results, it seems that the formation of solvated intercalates of TiS₂ could be considered as a strategy for improving divalent ion diffusion and consequently the overall reversibility of the redox process. On one hand, the expanded interlayer distances as well as the partial screening of the M²⁺ charge by the solvent molecules help diminish the interactions between the slabs and the highly polarizing divalent cations. This is in agreement both with previous theoretical studies showing that the diffusion barrier for Mg²⁺ between the layers progressively decreases when increasing *d*²² and our own DFT calculations confirming that the energy barrier decreases with the lower polarizing force of the divalent cation. On the other, a parallel with the specific case of Na insertion into graphite with glyme based electrolytes can be made, where solvated-Na⁺ intercalation (formation of ternary GIC) has been reported^{55,56} with very good cyclability.

Conclusions

In this study, we report on the electrochemical intercalation of Ca²⁺ and Mg²⁺ cations in layered TiS₂ using EC:PC (1:1 volume) mixture as electrolyte solvent. Fundamental understanding of the insertion process was acquired by in-depth SXR D structural analysis of the different new phases formed upon reduction of pristine TiS₂. The first phase, present both in Mg and Ca experiments, is found to be the result of a cation-solvated intercalation mechanism. In this co-intercalated phase, the M²⁺ cations enter the interlayer space keeping solvent molecule(s) in their proximity, leading to a substantial expansion of the lattice along the *c* axis. Differential absorption X-ray tomography results confirm Ca²⁺ intercalation inside TiS₂ particles. Full reversibility of the process was established through SXR D, thus this work represents a step forward towards the proof of concept of rechargeable Ca metal based batteries.

We speculate that the cation-solvated intercalation mechanism improves divalent cation migration inside the van der Waals gap between chalcogenide layers, as both the expanded interlayer space and the solvent-screened cation charge allow for lower diffusion barriers

when compared to energy barriers in conventional $M_x\text{TiS}_2$ intercalates ($M=\text{Ca}, \text{Mg}$). Further reduction of TiS_2 electrodes in Ca experiments leads to two different, possibly non co-intercalated, phases that form to the expense of unreacted TiS_2 , one being very similar to the $\text{Ca}_{0.5}\text{TiS}_2$ intercalate reported by Rouxel *et al.* and the other consistent with a second-stage $\text{Ca}_{0.16}\text{TiS}_2$ compound. In Mg experiments, no proof of the formation of these two phases has been found, and only a Mg^{2+} -solvated intercalate is growing upon TiS_2 reduction. This finding in conjunction with the possibility to form non co-intercalated phases in Ca experiments, may indicate that naked Mg^{2+} cannot be intercalated from EC:PC mixture due to the stronger solvent- Mg^{2+} interactions.

Acknowledgements

Authors acknowledge funding from Ministerio de Economía y Competitividad (Spain) for magnesium battery research (grant MAT2014-53500R). ICMAB's authors are also grateful for funding from Toyota Motor Europe for calcium battery research, for support through the "Severo Ochoa" Program for Centres of Excellence in R&D (SEV-2015-0496), to ALBA synchrotron for beam time allocation at MSPD beamline (proposal 2014070933) and to Dr. François Fauth for his assistance during data collection. The X-ray tomography experiments were performed at MISTRAL beamline at ALBA Synchrotron with the collaboration of ALBA staff and the ICMAB authors are grateful to Dino Tonti for helpful discussion. M.E. Arroyo-de Dompablo and N. Biskup acknowledge computational facilities from Universidad de Oviedo (MALTA-Consolider cluster).

Supporting Information

Electronic Supplementary Information (ESI): Figures S1-S4 (DFT calculations, simulated XRD, $\Delta\mu$ calculated sensibility) Table S1 (Rietveld refinement) and Video (3D distribution of $\Delta\mu$).

References

- ¹ Muldoon, J.; Bucur, C.B.; Gregory, T. Quest for Nonaqueous Multivalent Secondary Batteries: Magnesium and Beyond. *Chem. Rev.*, **2014**, 114, 11683.
- ² Canepa, P.; Gautam, G.S.; Hannah, D.C.; Malik, R.; Liu, M.; Gallagher, K.G.; Persson, K.A.; Ceder, G. Odyssey of Multivalent Cathode Materials: Open Questions and Future Challenges. *Chem. Rev.*, **2017**, 117, 4287.
- ³ Aurbach, D.; Lu, X.; Schechter, A.; Gofer, Y.; Gizbar, H.; Turgeman, R.; Cohen, Y.; Moshkovich, M.; Levi, E. Prototype systems for rechargeable magnesium batteries. *Nature*, **2000**, 407, 724.
- ⁴ Yoo, H.D.; Shterenberg, I.; Gofer, Y.; Gershinshy, G.; Pour, N.; Aurbach, D. Mg rechargeable batteries: an on-going challenge. *Energy Environ. Sci.*, **2013**, 6, 2265.
- ⁵ Ponrouch, A.; Frontera, C.; Bardé, F.; Palacín, M.R. Towards a calcium-based rechargeable battery. *Nat. Mater.*, **2016**, 15, 169.
- ⁶ Arroyo-de Dompablo, M.E.; Krich, C.; Nava-Avendaño, J.; Palacín, M.R.; Bardé, F. In quest of cathode materials for Ca ion batteries: the CaMO₃ perovskites (M = Mo, Cr, Mn, Fe, Co, and Ni). *Phys. Chem. Chem. Phys.*, **2016**, 18, 19966.
- ⁷ Arroyo-de Dompablo, M.E.; Krich, C.; Nava-Avendaño, J.; Biskup, N.; Palacín, M.R.; Bardé, F. A Joint Computational and Experimental Evaluation of CaMn₂O₄ Polymorphs as Cathode Materials for Ca Ion Batteries. *Chem. Mater.*, **2016**, 28, 6886.
- ⁸ Hayashi, M.; Arai, H.; Ohtsuka, H.; Sakurai, Y. Electrochemical Insertion/Extraction of Calcium Ions Using Crystalline Vanadium Oxide. *Electrochem. Solid State Lett.*, **2004**, 7, A119.
- ⁹ Bervas, M.; Klein, L.C.; Amatucci, G.G. Vanadium oxide–propylene carbonate composite as a host for the intercalation of polyvalent cations. *Solid State Ionics*, **2005**, 176, 2735.
- ¹⁰ Lipson, A.L.; Pan, B.; Lapidus, S.H.; Liao, C.; Vaughey, J.T.; Ingram, B.J. Rechargeable Ca-Ion Batteries: A New Energy Storage System. *Chem. Mater.*, **2015**, 27, 8442.
- ¹¹ Cabello, M.; Nacimiento, F.; Gonzalez, J.R.; Ortiz, G.; Alcantara, R.; Lavela, P.; Perez-Vicente, C.; Tirado, J.L. Advancing towards a veritable calcium-ion battery: CaCo₂O₄ positive electrode material. *Electrochem. Comm.*, **2016**, 67, 59.

-
- ¹² Proffit, D.L.; Fister, T.T.; Kim, S.; Pan, B.; Liao, C.; Vaughey, J.T. Utilization of Ca K-Edge X-ray Absorption Near Edge Structure to Identify Intercalation in Potential Multivalent Battery Materials. *J. Electrochem. Soc.*, **2016**, 163, A2508.
- ¹³ Whittingham, M.S. Chemistry of intercalation compounds: Metal guests in chalcogenide hosts. *Prog. Solid State Chem.*, **1978**, 12, 41.
- ¹⁴ Schöllhorn, R.; Meyer, H. Cathodic reduction of layered transition metal chalcogenides. *Mat. Res. Bull.*, **1974**, 9, 1237.
- ¹⁵ Lerf, A.; Schöllhorn, R. Solvation reactions of layered ternary sulfides A_xTiS_2 , A_xNbS_2 , and A_xTaS_2 . *Inorg. Chem.*, **1977**, 16, 2950.
- ¹⁶ Le Blanc-Soreau, A.; Rouxel, J. Facteurs physiques et structuraux dans les systèmes d'intercalaires : systèmes $A_x^{++}TiS_2$, cas du calcium. *C.R. Acad. Sc. Paris*, **1974**, 279, C303.
- ¹⁷ Gregory, T.; Hoffman, R.J.; Winterton, R.C. Nonaqueous Electrochemistry of Magnesium Applications to Energy Storage. *J. Electrochem. Soc.*, **1990**, 137, 775.
- ¹⁸ Novak, P.; Desilvestro, J. Electrochemical Insertion of Magnesium in Metal Oxides and Sulfides from Aprotic Electrolytes. *J. Electrochem. Soc.*, **1993**, 140, 140.
- ¹⁹ Bruce, P.G.; Krok, F.; Nowinski, J.; Gibson, V.C.; Tavakkoli, K. Chemical intercalation of magnesium into solid hosts. *J. Mater. Chem.*, **1991**, 1, 705.
- ²⁰ Amir, N.; Vestfrid, Y.; Chusid, O.; Gofer, Y.; Aurbach, D. Progress in nonaqueous magnesium electrochemistry. *J. Power Sources*, **2007**, 174, 1234.
- ²¹ Sun, X.; Bonnick, P.; Nazar, L.F. Layered TiS_2 positive electrode for Mg batteries. *ACS Energy Lett.*, **2016**, 1, 297.
- ²² Emily, A.; Van der Ven, A. Mg Intercalation in Layered and Spinel Host Crystal Structures for Mg Batteries. *Inorg. Chem.*, **2015**, 54, 4394.
- ²³ Yoo, H.D.; Liang, Y.; Dong, H.; Lin, J.; Wang, H.; Liu, Y.; Ma, L.; Wu, T.; Li, Y.; Ru, Q.; Jing, Y.; An, Q.; Zhou, W.; Guo, J.; Lu, J.; Pantelides, S.T.; Qian, X.; Yao, Y. Fast kinetics of magnesium monochloride cations in interlayer-expanded titanium disulfide for magnesium rechargeable batteries. *Nat. Comm.*, **2017**, 8, 339.

-
- ²⁴ Bian, X.; Gao, Y.; Fu, Q.; Indris, S.; Ju, Y.; Meng, Y.; Du, F.; Bramnik, N.; Ehrenberg, H.; Wei, Y. A long cycle-life and high safety Na⁺/Mg²⁺ hybrid-ion battery built by using a TiS₂ derived titanium sulfide cathode. *J. Mater. Chem. A*, **2017**, 5, 600.
- ²⁵ Ponrouch, A.; Palacín, M.R. On the impact of the slurry mixing procedure in the electrochemical performance of composite electrodes for Li-ion batteries: A case study for mesocarbon microbeads (MCMB) graphite and Co₃O₄. *J. Power Sources*, **2011**, 196, 9682.
- ²⁶ Tchitchekova, D.S.; Monti, D.; Johansson, P.; Bardé, F.; Randon-Vitanova, A.; Palacín, M.R.; Ponrouch, A. On the Reliability of Half-Cell Tests for Monovalent (Li⁺, Na⁺) and Divalent (Mg²⁺, Ca²⁺) Cation Based Batteries. *J. Electrochem. Soc.*, **2017**, 164, A1384.
- ²⁷ Thompson, A.H. Electrochemical Potential Spectroscopy: A New Electrochemical Measurement. *J. Electrochem. Soc.*, **1979**, 126, 608.
- ²⁸ Sorrentino, A.; Nicolás, J.; Valcárcel, R.; Chichón, F.J.; Rosanes, M.; Avila, J.; Tkachuk, A.; Irwin, J.; Ferrer, S.; Pereiro, E. MISTRAL: a transmission soft X-ray microscopy beamline for cryo nano-tomography of biological samples and magnetic domains imaging. *J. Synchrotron Radiat.*, **2015**, 22, 1112.
- ²⁹ Pereiro, E.; Nicolas, J.; Ferrer, S.; Howells, M. A soft X-ray beamline for transmission X-ray microscopy at ALBA. *J. Synchrotron Radiat.*, **2009**, 16, 505.
- ³⁰ Messaoudi, C.; Aschman, N.; Cunha, M.; Oikawa, T.; Sorzano, C.O.; Marco, S. Three-dimensional chemical mapping by EFTEM-TomoJ including improvement of SNR by PCA and ART reconstruction of volume by noise suppression. *Microsc. Microanal.*, **2013**, 19, 1669.
- ³¹ Kremer, J.R.; Mastronarde, D.N.; McIntosh, J.R. Computer Visualization of Three-Dimensional Image Data Using IMOD. *J. Struct. Biol.*, **1996**, 116, 71.
- ³² Conesa, J.J.; Otón, J.; Chiappi, M.; Carazo, J.M.; Pereiro, E.; Chichón, F.J.; Carrascosa, J.L. Intracellular nanoparticles mass quantification by near-edge absorption soft X-ray nanotomography. *Sci. Rep.*, **2016**, 6, 22354.
- ³³ Pettersen, E.F.; Goddard, T.D.; Huang, C.C.; Couch, G.S.; Greenblatt, D.M.; Meng, E.C.; Ferrin, T.E. UCSF Chimera—A visualization system for exploratory research and analysis. *J. Comput. Chem.*, **2004**, 25, 1605.

-
- ³⁴ Schneider, C.A.; Rasband, W.S.; Eliceiri, K.W. NIH Image to ImageJ: 25 years of image analysis. *Nat. Methods*, **2012**, *9*, 671.
- ³⁵ Kresse, G.; Furthmüller, E. Efficient iterative schemes for ab initio total-energy calculations using a plane-wave basis set. *J. Phys. Rev. B*, **1996**, *54*, 11169.
- ³⁶ Perdew, J.P.; Burke, K.; Ernzerhof, M. Generalized Gradient Approximation Made Simple. *Phys. Rev. Lett.*, **1996**, *77*, 3865.
- ³⁷ Bloch, P.E. Projector augmented-wave method. *Phys. Rev. B*, **1994**, *50*, 17953.
- ³⁸ Henkelman, G.; Uberuaga, B.; Jónsson, H. A climbing image nudged elastic band method for finding saddle points and minimum energy paths. *J. Chem. Phys.*, **2000**, *113*, 9901.
- ³⁹ Rong, Z.; Malik, R.; Canepa, P.; Gautam, G.S.; Liu, M.; Jain, A.; Persson, K.; Ceder, G. Materials design rules for multivalent ion mobility in intercalation structures. *Chem. Mater.*, **2015**, *27*, 6016
- ⁴⁰ Van der Ven, A.; Thomas, J.C.; Xu, Q.; Swoboda, B.; Morgan, D. Nondilute diffusion from first principles: Li diffusion in Li_xTiS_2 . *Phys. Rev. B*, **2008**, *78*, 104306; Wilkening, M.; Heitjans, P. Li jump process in $\text{h-Li}_{0.7}\text{TiS}_2$ studied by two-time ^7Li spin-alignment echo NMR and comparison with results on two-dimensional diffusion from nuclear magnetic relaxation. *Phys. Rev. B*, **2008**, *77*, 024311.
- ⁴¹ Persson, K.; Hinuma, Y.; Meng, Y.S.; Van der Ven, A.; Ceder, G. Thermodynamic and kinetic properties of the Li-graphite system from first-principles calculations. *Phys. Rev. B*, **2010**, *82*, 125416.
- ⁴² Kang, K.; Ceder, G. Factors that affect Li mobility in layered lithium transition metal oxides. *Phys. Rev. B*, **2006**, *74*, 094105.
- ⁴³ Samad, A.; Shafique, A.; Shin, Y.H. Adsorption and diffusion of mono, di, and trivalent ions on two-dimensional TiS_2 . *Nanotechnology*, **2017**, *28*, 175401.
- ⁴⁴ McTaggart, F.K.; Wadsley, A. The sulphides, Selenides, and Tellurides of Titanium, Zirconium, Hafnium, and Thorium. II. Chemical properties. *Aust. J. Chem.*, **1958**, *11*, 445.
- ⁴⁵ Chianelli, R.; Scanlon, J.; Whittingham, M.; Gamble, F. Structural studies of the intercalation complexes titanium sulfide-ammonia ($\text{TiS}_2 \cdot \text{NH}_3$) and tantalum sulfide-ammonia ($\text{TaS}_2 \cdot \text{NH}_3$). *Inorg. Chem.*, **1975**, *14*, 1691-1696.
- ⁴⁶ McKelvy, M.; Bernard, L.; Glaunsinger, W.; Colombet, P. Ammonia oxidation and charge compensation in the metal ammonia intercalates $\text{Li}^+_x(\text{NH}_4^+)_y(\text{NH}_3)_z\text{TiS}_2^{(x+y)-}$. *J. Solid State Chem.*, **1986**, *65*, 79-88.

-
- ⁴⁷ Young Jr., V.G.; McKelvy, M.J.; Glaunsinger, W.S.; Von Dreele, R.B. Structural investigation of lithium-ammonia intercalation compounds of titanium sulfide (TiS₂). *Chem. Mater.*, **1990**, *2*, 75-81.
- ⁴⁸ Schöllhorn, R.; Zagefka, H.; Butz, T.; Lerf, A. Ionic bonding model of the pyridine intercalation compounds of layered transition metal dichalcogenides. *Mater. Res. Bull.*, **1979**, *14*, 369.
- ⁴⁹ Schöllhorn, R.; Zagefka, H.D. Demonstration of the Ionic Structure of the Intercalation Compound TaS₂ · NH₃. *Angew. Chem. Int. Ed. in English*, **1977**, *16*, 199.
- ⁵⁰ Schöllhorn, R. Intercalation chemistry. *Physica B+C*, **1980**, *99*, 89.
- ⁵¹ Radin, M.D.; Van der Ven, A. Stability of Prismatic and Octahedral Coordination in Layered Oxides and Sulfides Intercalated with Alkali and Alkaline-Earth Metals. *Chem. Mater.*, **2016**, *28*, 7898.
- ⁵² Bouwmeester, H.; Dekker, E.; Bronsema, K.; Haange, R.; Wiegers, G. *Chemischer Informationsdienst*, **1983**, *14* (10).
- ⁵³ Shakourian-Fard, M.; Kamath, G.; Sankaranarayanan, S.K.R.S. Electronic Structure Insights into the Solvation of Magnesium Ions with Cyclic and Acyclic Carbonates. *Chem. Phys. Chem.*, **2015**, *16*, 3607.
- ⁵⁴ Xu, K. Nonaqueous Liquid Electrolytes for Lithium-Based Rechargeable Batteries. *Chem. Rev.*, **2004**, *104*, 4303.
- ⁵⁵ Jache, B.; Adelhelm, P. Use of Graphite as a Highly Reversible Electrode with Superior Cycle Life for Sodium-Ion Batteries by Making Use of Co-Intercalation Phenomena. *Angew. Chem. Int. Ed.*, **2014**, *53*, 10169.
- ⁵⁶ Kim, H.; Hong, J.; Yoon, G.; Kim, H.; Park, K.Y.; Park, M.S.; Yoon, W.S.; Kang, K. Sodium intercalation chemistry in graphite. *Energy Environ. Sci.*, **2015**, *8*, 2963.